*Int. J. Electrochem. Sci.*, 13 **(2018)** 5041 – 5053, doi: 10.20964/2018.05.19

International Journal of
ELECTROCHEMICAL
SCIENCE
www.electrochemsci.org

# Fabrication of Tungsten Trioxide-loaded Titania Nanotubes as a Potential Photoanode for Photoelectrochemical Cell

*Nur Farah Atikah binti Harun,*[1] *Yusairie bin Mohd,*[1] *Lim Ying Pei,*[2] *Lim Ying Chin* [1*]

[1] School of Chemistry and Environment, Faculty of Applied Sciences, Universiti Teknologi MARA, Shah Alam, 40450 Selangor, Malaysia.
[2] Faculty of Chemical Engineering, Universiti Teknologi MARA, Shah Alam, 40450 Selangor, Malaysia.
[*]E-mail: limyi613@salam.uitm.edu.my

*Received:* 23 November 2017 / *Accepted:* 28 February 2018 / *Published:* 10 April 2018

This study aimed to investigate the effect of deposition potential on the growth of tungsten trioxide electrodeposited onto titania nanotubes (WTNT) in a fixed solution pH of 1.5 as well as its effect on the photoelectrochemical (PEC) properties of titania nanotubes (TNT). Well-ordered crystalline TNT and WTNT were obtained via anodization of titanium foil and electrodeposition of $WO_3$ species respectively as proven via FESEM, EDX, and XRD analyses. All WTNTs showed enhanced PEC performance compared to the blank TNT. WTNT/–0.65 V prepared under deposition potential at –0.65 V exhibited the highest PEC performance (Ƞ = 9.63 %) compared to other WTNTs and almost 6 times higher compared to blank TNT (Ƞ = 1.65 %). Such enhancement was due to optimal amount and morphology of tungsten trioxide deposited which enabled efficient synergetic effect between tungsten trioxide and TNT.

**Keywords:** charge transport, electrodeposition, nanocomposites, titania nanotubes, photoelectrochemistry

## 1. INTRODUCTION

Current energy demands and unsolved environmental problems have forced humankind to search for greener alternatives. The advancements of today's technology provide the ideas and ways in which energy can be gained without depleting and causing adverse effects towards the environment. Therefore, renewable energy resources are becoming of great interest. One of the attractive methods to use renewable energy resources is by utilizing materials, such as semiconductors that are capable of generating energy (for example, electricity). Titanium dioxide ($TiO_2$) has become one of the most popular semiconductors being utilized for various photo-induced applications, such as in photoelectrochemical cells (PEC).

Chemical stability, good photo reactivity, appropriate band gap energy (1.23 eV) that surpasses the thermodynamic potential of water splitting [1] and environmentally friendly, make $TiO_2$ a suitable material to be used as an electrode in a PEC cell. However, its low quantum efficiency and high recombination rate of charge carriers [2] would be disadvantageous for this application. Furthermore, the wide band gap of $TiO_2$ ($E_g$ = 3.2 eV for $TiO_2$ anatase) [3] consequently makes it only UV-reactive [4], whilst a suitable material that can harvest broader light spectrum is highly recommended if high PEC performance is desired.

Current researches highlight the improved performance of various photo-induced applications involving $TiO_2$ upon various modifications to overcome its disadvantages. This includes surface modifications such as transforming bulk $TiO_2$ into nanotubular titania (TNT). Other low band gap semiconductors have been proposed which offer reduced band gap energy and enhanced visible light reactivity, such as the introduction of noble metals[5-7], metals [2,8], and metal oxides[9, 10]. Among these semiconductor materials, tungsten trioxide showed promising results at lowering the band gap energy of TNT due to its narrow band gap ($E_g$ = 2.4–2.8 eV) [10] which enables TNT to absorb more visible light energy [11] and hence enhancing PEC performance.

Numerous synthesis methods have been conducted to load $WO_3$ onto TNTs via different methods such as chemical bath deposition (CBD) [12, 13], hydrothermal method [14], and single-step anodization [15, 16]. Deposition of $WO_3$ via electrodeposition was conducted by Martins and co-workers [11], by studying the effect of deposition time at a specific deposition potential of –0.45 V versus saturated calomel electrode (SCE). Nonetheless, reports on depositing $WO_3$ onto TNT (WTNT) via the electrodeposition method are still lacking even though electrodeposition method has the advantage of easy control of film thickness [11] which can be accomplished by adjusting the deposition potentials and other related parameters, such as solution pH [17]. Therefore, other parameter such as the effect of deposition potential is yet to be investigated. Hence, this study aimed to develop a facile way to deposit tungsten trioxide onto titania nanotubes. This study also aimed to investigate the effects of deposition potential on the growth of $WO_3$ on TNT, the photoelectrochemical properties, light spectrum absorption behaviour and band gap energy of the fabricated WTNTs.

## 2. EXPERIMENTAL

### *2.1. Preparation of titania nanotubes (TNT)*

The preparation of TNT was as follows: a titanium foil was cut into 2.0×1.0 $cm^2$ and ultrasonically cleaned in 2-propanol followed by acetone and distilled water for 15 minutes each. The blank TNT was prepared via the anodization of Ti as described by Lim and co-workers [8]. The anodization process was conducted in a two-electrode system at 40 V at room temperature. A mixture of 9:1 vol.% of ethylene glycol to distilled water, containing 0.5 wt.% of $NH_4F$ was anodized for 60 minutes using a high-density graphite as the cathode and the titanium foil as the anode. The two electrodes were located at a fixed distance of 2 cm to ensure the application of constant electric field [19]. All chemicals were purchased from Sigma Aldrich and no further purification was made prior to

usage. Finally, the as-anodized TNTs were annealed in air at 500 °C with 2 °C/min ramp for 2 hours.

### *2.2. Preparation of tungsten trioxide-loaded titania nanotubes (WTNT)*

WTNTs were prepared via electrodeposition using a three-electrode electrochemical cell where a platinum wire served as the counter electrode, Ag/AgCl as the reference electrode and the previously prepared TNT as the working electrode as well as a template for the deposition of $WO_3$. The electrodes were immersed in 50 mL of 2.5 mM $Na_2WO_4$. The solution was adjusted to pH 1.5 by adding 1.4 mL of $H_2O_2$ and $HNO_3$ dropwise. The deposition potential was varied from –0.30, –0.45, –0.55, –0.65, and –0.75 V while keeping the deposition time constant at 15 minutes for each sample.

### *2.3. Characterization of tungsten trioxide-loaded titania nanotubes*

The blank TNT and WTNT samples prepared under various deposition potentials were characterized to determine their physicochemical properties. FESEM morphological analysis and EDX elemental composition analysis were conducted using a Carl Zeiss SUPRA 40VP electron microscope. XRD analysis was conducted to examine the crystal structure of the samples using the X'Pert Pro-MPD, PANalytical diffractometer, operating at 40 kV and 30 mA, with a scanning range of $2\theta = 10–90°$ using Cu Kα ($\lambda$ = 1.504Å). UV-DRS analysis was conducted using the UV-Vis-NIR spectrophotometer (Model: UV 3600, Shimadzu Corporation, Kyoto, Japan) at wavelength range of 200–800 nm to observe the effect of doping $WO_3$ on the optical properties of TNT.

The photoelectrochemical properties of all samples were investigated via a photoelectrochemical (PEC) test in a three-electrode cell equipped with a flat quartz window. The prepared sample was used as the working electrode, a platinum wire as the counter electrode and Ag/AgCl as the reference electrode which were immersed in a mixture of 0.1 M $Na_2SO_4$ and 2 M $C_2H_5OH$. The current was measured using a potentiostat (AUTOLAB) and scanned using a potential sweep from +1 to −1 V with a sweep rate of 50 mV/s. The photocurrent was measured under irradiation from a 150 mW/cm$^2$ halogen lamp placed 15 cm away from the cell which passed through the quartz window during the potential sweep while dark current was measured without the irradiation.

## 3. RESULTS AND DISCUSSION

### *3.1. Electrodeposition of tungsten trioxide onto titania nanotubes*

A cyclic voltammetric (CV) analysis was conducted prior to the chronoamperometric deposition of tungsten trioxide onto TNTs to determine the probable potential range for the electrodeposition process. Figure 1 presents the cyclic voltammogram obtained in a typical three-electrode system over a range of +0.2 V to –1.0 V. This potential range was selected because the reduction of tungstate ion into $WO_3$ was expected to take place in this potential region in the electrolyte as previously mentioned in Section 2.2. For comparison purposes, a CV analysis was also

conducted in a blank solution. This solution consisted of 50 mL deionized water, 1.4 mL $H_2O_2$ and $HNO_3$ which was added dropwise to obtain pH of 1.5.

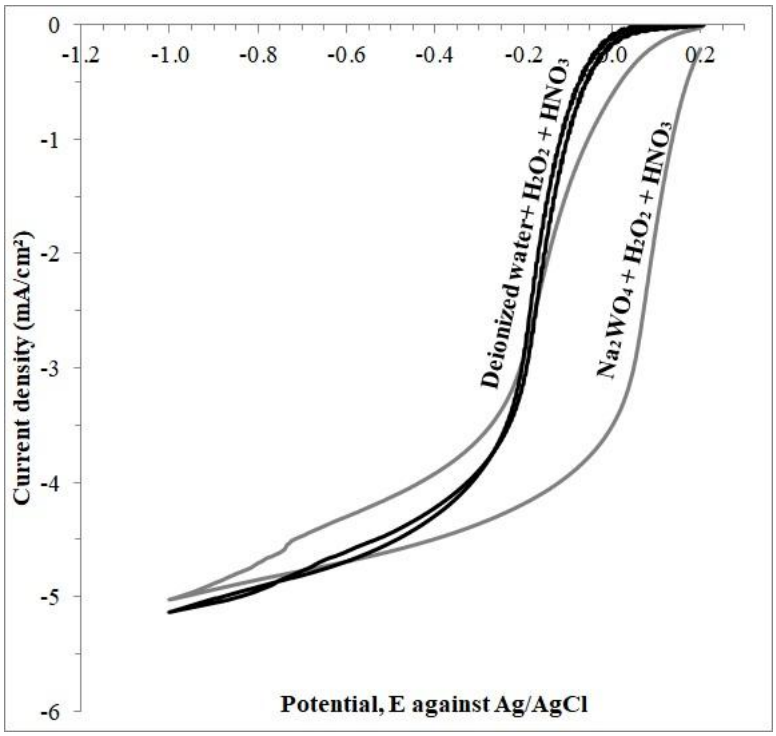


**Figure 1**. Cyclic voltammograms at 50 mV/s of TNT in $Na_2WO_4/H_2O_2/HNO_3$ solution and in a blank solution of deionized water/$H_2O_2/HNO_3$ of pH 1.5 each.

Upon an applied potential, the TNT would be supplied with electrons, and the tungstate ions in the electrolyte would move towards the TNT. In the presence of $H^+$ ions and $H_2O_2$, electron transport would occur at the electrode/electrolyte interface. Hence, the cation species would be step-wisely reduced into solid $WO_3$ species which would be deposited onto the TNT surface. The possible reactions are given by the following Equations (1) and (2) [11]:

$$2H^+ + 2WO_4^{2-} + 4H_2O_2 \rightarrow W_2O_{11}^{2-} + 5H_2O \quad (1)$$

$$2H^+ + W_2O_{11}^{2-} \rightarrow 2WO_3 + 2O_2 + H_2O \quad (2)$$

From the backward (cathodic) scan of the cyclic voltammogram, the electrochemical reaction for the electroactive species occurred at approximately +0.2 V where the electrodeposition process was controlled by the electron transfer process [20]. Then, it accelerated to –0.3 V before a gradual current increment was observed up to –1.0 V. The rapid current increment that occurred in the potential range between +0.2 V to –0.3 V indicated the electron transport reaction where electrons from the TNT were rapidly supplied to reduce the tungstate ions into $WO_3$ particles. The mass transport was controlled at a potential range of –0.3 V to –1.0 V whereby the current was observed to increase slowly. It was understood that higher applied current would result in a faster electrodeposition rate. Therefore, the probable potential range was chosen between –0.30 V and –0.75 V for the potentiostatic deposition of $WO_3$ onto TNT.

*3.2. Morphological and elemental composition of WTNT*

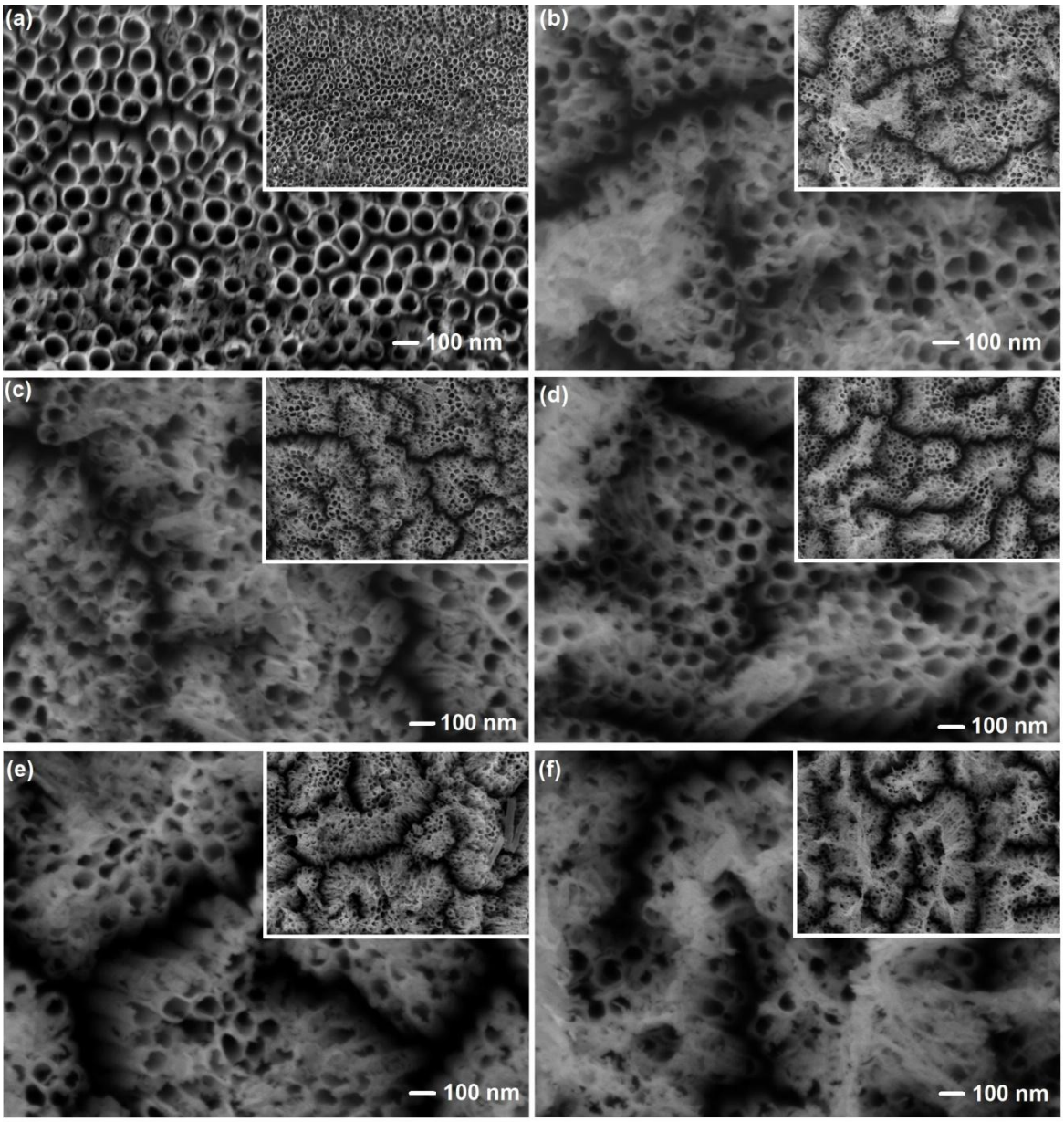


**Figure 2.** FESEM images of: (a) blank TNT; (b) WTNT/–0.30 V; (c) WTNT/–0.45 V; (d) WTNT/–0.55 V; (e) WTNT/–0.65 V; and (f) WTNT/–0.75 V at 50,000 magnification. Inset figures are FESEM images at 20,000 magnification.

In order to investigate the effect of deposition potential on the growth of $WO_3$ on TNTs and the amount of tungsten deposited, FESEM and EDX analyses were conducted. Figure 2 shows FESEM images of the blank TNT and WTNTs prepared under various deposition potentials. Titania nanotubes with outer diameter that ranged between 107 and 143 nm and inner diameter that ranged between 78 and 104 nm were successfully obtained after anodization. Upon applying the potential on the smooth Ti foil and in the presence of water molecules, the Ti foil was oxidized into $TiO_2$. Then, fluoride ions (from $NH_4F$) reacted with $TiO_2$ to form a complex of $TiF_6^{2-}$ which is soluble and stable in the fluoride-

containing electrolyte [21]. The soluble complex was then washed, leaving behind pits on the $TiO_2$ surface [2]. With longer anodization time, the pits gradually became nanosized tubes. The overall chemical reaction as reported by Yoriya and co-workers [21] is shown by Equation (3):

$$TiO_2 + 6F^- + 4H^+ \rightarrow TiF_6^{2-} + 2H_2O \quad (3)$$

From Figure 2, irregular particles were observed to be deposited on all WTNT samples presumably in the form of tungsten trioxide. This was proven by the presence of tungsten in the EDX analysis as listed in Table 3, hence indicating that the fabrication of WTNT via electrodeposition was a success. For the WTNT/–0.30 V sample, tungsten trioxide particles were aggregated and had randomly covered the nanotubes' mouths and the TNTs were slightly clumped together upon electrodeposition. WTNT/–0.45 V and WTNT/–0.55 V samples exhibited similar morphology and a comparable amount of tungsten trioxide was deposited on both samples as shown by the EDX analysis (Table 3). This could be attributed to the similar cathodic current applied in this potential region (Figure 1).

As for the WTNT/–0.65 V sample, a high amount of tungsten trioxide with small flake-like shapes was seen to cover the top mouth of the nanotubes without aggregation. This could be an advantage in PEC application since tungsten trioxide has a uniformed contact with the $TiO_2$ nanotubes. As such, this could possibly promote the synergetic effect between tungsten trioxide and TNT. However, in the WTNT/–0.75 V sample, the amount of deposited tungsten trioxide seemed to be comparable to that of WTNT/–0.30 V and WTNT/–0.55 V but with severe aggregation. This condition is undesirable since it could possibly result in lesser light penetration and absorption by the WTNT during PEC test and thus lowers the PEC performance of the WTNT.

### *3.3. Crystal structure of WTNT using XRD analysis*

It was anticipated that the deposition potentials could affect the deposition behaviour and morphology of WTNT as well as affect the crystal structure of the samples. Therefore, XRD analysis was conducted to evaluate the crystallinity and crystal structure of the WTNT samples. The resulting diffractograms are presented in Figure 3 and the crystallographic analysis data are tabulated in Table 1.

Based on the XRD patterns of the TNT and WTNT samples, crystalline TNT was successfully fabricated upon anodization and annealing. The blank TNT and the WTNT samples exhibited Ti diffraction peaks (JCPDS 44-1294) at $2\theta$ = 35.2º, 38.4º, 40.3º, 53.1º, 62.9º, 70.7º, 74.1º, 77.2º, 82.3º, and 86.8º corresponding to (100), (002), (101), (102), (110), (103), (112), (201), (004), and (202) planes, respectively.

In addition, the TNT and WTNT samples had shown a prominent characteristic anatase peak (JCPDS 21-1272) at $2\theta$ = 25.4˚ corresponding to the (101) plane as listed in Table 1. The anatase $TiO_2$ crystallite size (D) of the blank TNT and all WTNT samples had ranged between 10 and 13 nm (Table 1). Other anatase peaks could also be observed at $2\theta$ = 48.0º, 53.7º, 55.1º, and 68.7º, which corresponded to the (200), (105), (211), and (116) planes respectively. A small rutile peak at $2\theta$ = 27.4º was also observed which corresponded to the (110) plane (JCPDS 21-1276). These results showed that the deposited TNT has a mixture of anatase and rutile structures. The major anatase $TiO_2$ phase would be beneficial in terms of better PEC performance compared to the rutile phase. This is because better

electron mobility can be achieved in anatase $TiO_2$ compared to in rutile [1].

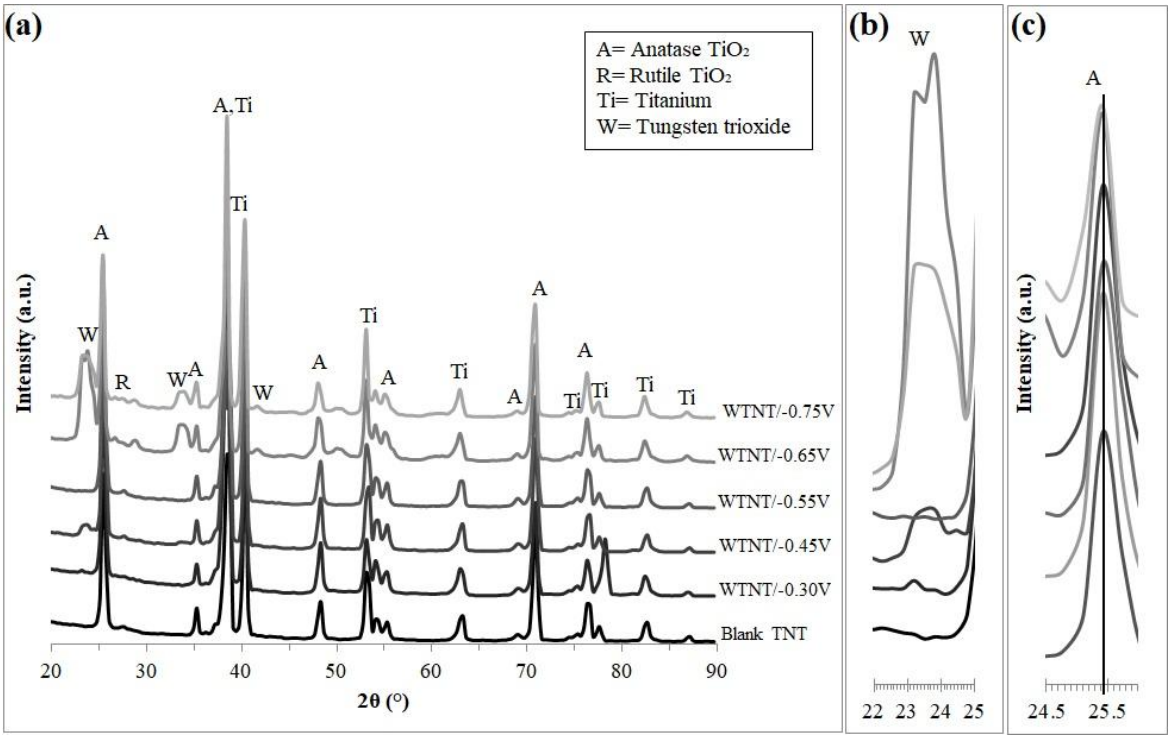


**Figure 3**. (a) XRD diffractograms for blank TNT and WTNT samples prepared under various deposition potentials. Small figures attached are the zoom-in figures: (b) 2θ = 22-25º, where the prominent tungsten trioxide peaks were detected, and (c) 2θ = 24.5-26º, where the prominent anatase $TiO_2$ peaks were exhibited.

Upon the deposition of tungsten trioxide, prominent characteristic peaks of monoclinic $WO_3$ (*m*-$WO_3$) at 2θ = 23.2º could be observed in all WTNT samples as shown in Figure 3b and Table 1. WTNT/−0.30 V, WTNT/−0.45 V, WTNT/−0.65 V and WTNT/−0.75 V possessed *m*-$WO_3$ (JCPDS 43-1035) with overlapping doublet peaks at 2θ = 23.2º and 23.5º which corresponded to the (002) and (020) planes respectively. Meanwhile, WTNT/−0.55 V exhibited a single *m*-$WO_3$ peak at 23.5˚. The growth of *m*-$WO_3$ in all WTNT samples could be attributed to the post-calcination process which was conducted at a favourable temperature of 500 °C as reported in several references[22, 23]. It was expected that the electrodeposition of tungsten trioxide which was conducted at pH 1.5, could yield other crystalline structures, such as orthorhombic tungsten trioxide (*o*-$WO_3$), as reported by Marques and co-workers [24]. It was reported that *o*-$WO_3$ nanoparticles were obtained from $Na_2WO_4.2H_2O$ and NaCl solution under pH 1.8. However, no other crystalline structures for tungsten trioxide were observed in the diffractograms, suggesting that solution pH has no effect on the crystal structure of the electrodeposited tungsten trioxide onto TNT.

It is possible that some of the $WO_3$ particles have been diffused into the $TiO_2$ lattice due to the similar radius between $W^{6+}$ and $Ti^{4+}$ [10], and the similarity in bond length of W-O and Ti-O [25]. To confirm these possibilities, several issues should be considered such as the shifting of the prominent anatase $TiO_2$ peak, the changing lattice constant or the cell volume of the anatase $TiO_2$ that resulted

from the electrodeposition of $WO_3$ onto TNT. Therefore, crystallographic analysis was conducted on WTNT samples to study the incorporation of $W^{6+}$ into $TiO_2$ lattice. The resulting crystallographic data are presented in Table 1. The lattice constants (*a* and *c*) of the anatase $TiO_2$ peaks as well as the cell volume (V) were obtained from the Rietveld refinement of the resulting spectra using X'Pert HighScore Plus. The cell volume of anatase $TiO_2$ was calculated by considering its tetragonal system, where $a = b \neq c$, using the following Equation (4):

$$V = a^2c \quad (4)$$

The crystallite size of anatase $TiO_2$ present in WTNT samples was calculated using the following Scherrer equation, as reported by Nadzirah and co-workers [26]:

$$D = 0.9\lambda/\beta\cos\theta \quad (5)$$

Where λ refers to the wavelength of X-ray used (1.504 Å), β refers to the full width at half maximum (FWHM) of the XRD peak and θ refers to the Bragg's angle.

Based on Figure 3c and the 2θ list in Table 1, there was no obvious shifting of anatase peak at $2\theta = 25.4^{\circ}$ for all WTNT samples, suggesting that $WO_3$ was not incorporated into $TiO_2$ lattice in these samples. This observation is supported by the crystallographic analysis data shown in Table 1 where there was no obvious change neither in the lattice constant (*a*) nor in the expansion of the cell volume for all WTNT samples.

**Table 1.** The 2θ of anatase $TiO_2$ at diffraction plane [101], crystallite size of anatase $TiO_2$, lattice constants, *a* and *c* of $TiO_2$, unit cell volume of anatase $TiO_2$, 2θ of $WO_3$ and the crystal structure of electrodeposited $WO_3$

| **Samples** | **2θ of anatase $TiO_2$ (°)** | **D (nm)** | ***a* (Å)** | ***c* (Å)** | **V (Å)** | **$WO_3$ structure** | **$WO_3$ plane [hkl]** | **2θ (°)** |
|---|---|---|---|---|---|---|---|---|
| Blank TNT | 25.4 | 10.1 | 3.76 | 9.62 | 136.3 | No peak | | |
| WTNT/–0.30 V | 25.4 | 10.1 | 3.77 | 9.59 | 136.7 | *m*-$WO_3$ | [002] | 23.2 |
| | | | | | | *m*-$WO_3$ | [020] | 23.5 |
| WTNT/–0.45 V | 25.5 | 12.2 | 3.77 | 9.55 | 135.4 | *m*-$WO_3$ | [002] | 23.2 |
| | | | | | | *m*-$WO_3$ | [020] | 23.5 |
| WTNT/–0.55 V | 25.4 | 10.1 | 3.77 | 9.64 | 136.9 | *m*-$WO_3$ | [020] | 23.5 |
| WTNT/–0.65 V | 25.5 | 13.0 | 3.77 | 9.57 | 136.0 | *m*-$WO_3$ | [002] | 23.2 |
| | | | | | | *m*-$WO_3$ | [020] | 23.5 |
| WTNT/–0.75 V | 25.4 | 10.1 | 3.78 | 9.55 | 136.3 | *m*-$WO_3$ | [002] | 23.2 |
| | | | | | | *m*-$WO_3$ | [020] | 23.5 |

### *3.4. Photoelectrochemical properties of WTNT*

The effect of tungsten trioxide deposition on the photoelectrochemical properties of TNT was examined via a PEC test. In this study, the transient photocurrent responses were scanned from +1 V to –1 V, both with and without illumination to measure the photocurrent and dark current. The photoconversion efficiency, Ƞ (%) was calculated using Equation (6):

$$\eta = \frac{I_o(1.23 - V_{bias})}{J_{light}} \times 100 \quad (6)$$

where $I_o$ refers to the photocurrent density ($A/m^2$), 1.23 V is the water splitting theoretical potential, $V_{bias}$ is the applied external potential (V) and $J_{light}$ is the light irradiance ($W/m^2$). The photoresponses and the photoconversion efficiency values for blank TNT and all WTNT samples are graphically presented in Figure 4. The additional photoelectrochemical data are tabulated in Table 2.

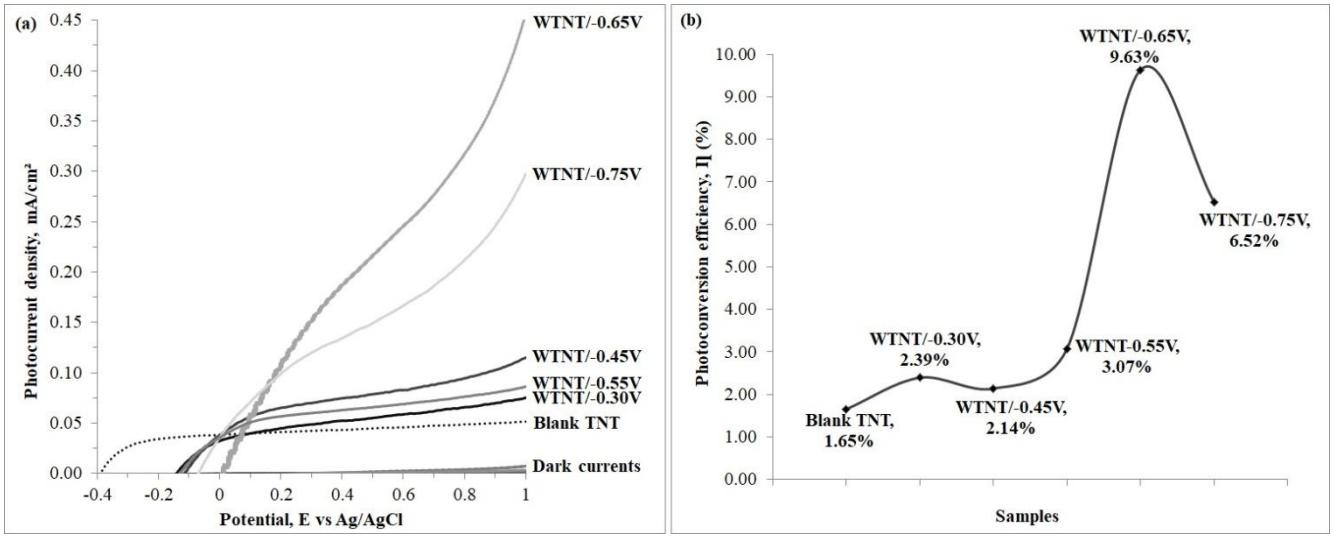


**Figure 4.** (a) Photoresponses obtained from potential sweep at 50 mV/s in 0.1 M $Na_2SO_4$ + 2 M $C_2H_5OH$ electrolyte under 150 $mW/cm^2$ light illumination; and (b) trends of photoconversion efficiency performances of blank TNT and WTNT samples prepared under various deposition potentials. The photoconversion efficiency values were calculated at $V_{bias}$ = +0.7 V

**Table 2.** Photoelectrochemical data of blank TNT and WTNT samples prepared at different deposition potentials. The photocurrent densities were calculated at $V_{bias}$ = +0.7 V

| Samples | $E_{oc}$ (mV) | Photocurrent density, mA/cm² |
|---|---|---|
| Blank TNT | –389.1 | 0.4690 |
| WTNT/–0.30 V | –140.1 | 0.6801 |
| WTNT/–0.45 V | –113.2 | 0.6078 |
| WTNT–0.55 V | –127.9 | 0.8722 |
| WTNT/–0.65 V | +3.967 | 2.738 |
| WTNT/–0.75 V | –66.83 | 1.854 |

The PEC performances of all WTNT samples were observed to increase upon the electrodeposition of tungsten trioxide onto TNT which was similar to the observation made by Martins and co-workers [11]. This observation is supported by their enhanced photoresponses (Figure 4a), higher overall photoconversion efficiency values (Figure 4b) and higher photocurrent densities (Table 2) compared to blank TNT. Dark current was almost zero and thus negligible for all samples, indicating that the fabricated samples were photoreactive.

The $E_{oc}$ of the blank TNT was observed to have shifted towards more positive potentials and the extent of shifting was seen to be directly proportional to the amount of tungsten present (Table 2). In the WTNT/–0.65 V sample where the highest amount of tungsten was deposited (as shown by the EDX analysis), the $E_{oc}$ started at a positive potential of +3.967 mV. This might be explained by the n-type semiconductor possessed by $WO_3$ whereby water splitting for this type of material tends to start at positive potentials, as proven by Jeffery and co-workers. [27]. Another reason might be explained by the fact that the introduction of $WO_3$ has increased the energy barrier at the WTNT electrode-electrolyte interface which possibly reduce the back-electron transfer from the CB of TNT [28].

The highest PEC performance was shown by the WTNT/–0.65 V sample with a photoconversion efficiency of 9.63% which was six times higher compared to TNT (Ƞ = 1.66%). The higher photoconversion efficiency and photocurrent density of WTNTs which were calculated at higher potentials further proved the n-type semiconducting behaviour of tungsten trioxide where the application of higher bias potentials had resulted in efficient electron-hole separation [27]. Consequently, photogenerated electron-hole recombination was hindered [29]. Such efficient electron-hole separation could be attributed to the band gap narrowing effect induced by $WO_3$ on the TNT. As such, UV-DRS analysis was conducted to support this assumption.

### *3.4. Optical property analysis of TNT and WTNT samples using UV-DRS*

A UV-DRS analysis was conducted on the blank TNT and the WTNT samples to provide some insights on the synergetic effect between $WO_3$ and the $TiO_2$ nanotubes. Figure 5a shows the UV-DR spectra of all samples while Figure 5b depicts the Tauc plot derived from the reflectance spectra of the TNT and the WTNT/–0.65 V sample. These plots were used to obtain the optical band gap energy which was derived using the following Equation (7) [30] where indirect band transitions were assumed.

$$\alpha h\nu = A(h\nu - E_g)^{1/2} \qquad (7)$$

The strong UV light absorbance at $\lambda < 380$ nm, shown by the pristine TNT and all WTNT samples confirmed the absorption of $TiO_2$ due to its UV-light reactive properties [31]. Nonetheless, WTNT samples had exhibited stronger UV light absorption compared to blank TNT. This result shows that tungsten trioxide could also exhibit UV light reactivity as supported by other findings with similar observations [11]. Improvement of visible light absorption was also observed in all WTNT samples consistent with other reports [14] as shown by the higher absorption intensities at $\lambda > 380$ nm compared to blank TNT in the inset of Figure 5a. This observation suggests a broader utilization of light spectrum in both UV and visible light region for WTNTs.

The resulting band gap for the blank TNT was 3.0 eV, which was agreeable with other findings [2]. However, the current band gap recorded was lower than most reports ($E_g$ = 3.2 eV) for major anatase $TiO_2$ nanotubes [32-36] which was due to the presence of the rutile phase, as proven by the XRD analysis. The UV light absorption edge for WTNT/–0.30 V, WTNT/–0.45 V, WTNT/–0.55 V, and WTNT/–0.75 V did not seem to shift from that of blank TNT as shown in Figure 5a. Consequently, similar $E_g$ values were obtained (3.0 eV) for these samples and blank TNT. This result

suggests that the amount of tungsten trioxide at these potentials was insufficient and hence did not significantly alter the $E_g$ of blank TNT. Among these samples, WTNT/−0.65 V had shown an obvious red-shifting of the absorption edge as reported by previous works [14, 15, 37] resulting in a greatly narrowed $E_g$ of 2.5 eV. This could be attributed to the high amount of tungsten trioxide in the sample which had sufficiently narrowed down the $E_g$ of blank TNT. Thus, the deposited $WO_3$ on the TNT surface had introduced an impurity level between the valence band and the conduction band of $TiO_2$ to introduce such effect [10].

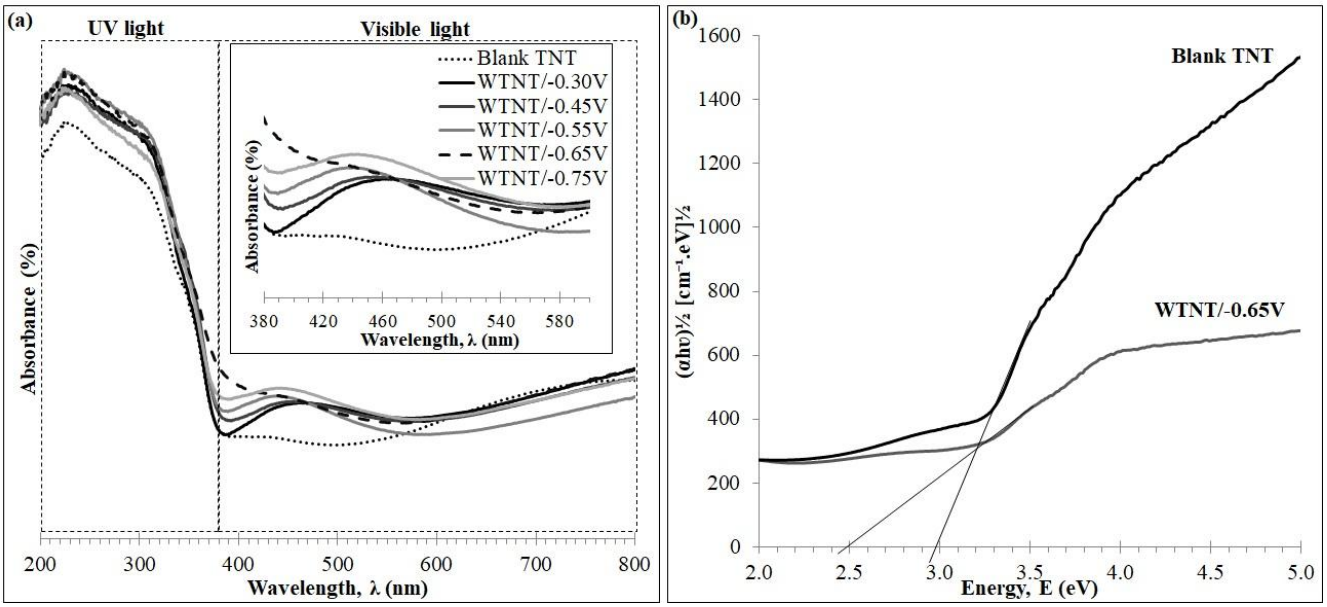


**Figure 5.** (a) UV-DR spectra of all samples, with inset zoom-in of spectra for wavelengths between 380-600 nm; and (b) Tauc plots derived from the reflectance spectra of blank TNT and WTNT/−0.65 V with the assumption of indirect band transitions

**Table 3.** Band gap energy of TNT and WTNT samples, and the corresponding amount of tungsten

| Samples | Amount of W (wt.%) | Amount of W (at.%) | Band gap energy, $E_g$ (eV) |
|---|---|---|---|
| Blank TNT | 0.00 | 0.00 | 3.0 |
| WTNT/−0.30 V | 6.64 | 1.01 | 3.0 |
| WTNT/−0.45 V | 6.06 | 0.90 | 3.0 |
| WTNT−0.55 V | 4.60 | 0.69 | 3.0 |
| WTNT/−0.65 V | 24.23 | 4.29 | 2.5 |
| WTNT/−0.75 V | 5.27 | 0.76 | 3.0 |

Nevertheless, the low amount of tungsten detected in other WTNT samples, apart from WTNT/−0.65 V was sufficient to enhance the photoelectrochemical performance of TNT. This observation was supported by findings made by Momeni [38] who reported that the photocatalytic activity of WTNT samples was enhanced even though the amount of tungsten detected by EDX was even lower than presently recorded.

Therefore, the enhanced performance of WTNT/–0.65 V could be explained by the possible synergetic effect possessed by both chemical species. First, the visible light reactive $WO_3$ deposited onto the UV light reactive TNT had enabled a broader utilization of light spectrum. In other words, more sunlight could be harvested. Second, the narrow band-gap of $WO_3$ deposited onto the TNT has narrowed down the $E_g$ due to an impurity level introduced between the valence band and the conduction band of $TiO_2$. This condition consequently improved the photogenerated charge separation and reduced the recombination rate of charge carriers, hence boosting the PEC performance of the WTNT samples. Nevertheless, the enhanced PEC performance was not based on the high amount of tungsten trioxide deposited. The distribution and morphology of $WO_3$ on the TNT had allowed better light penetration. Meanwhile, the crystallinity of the samples had allowed good electron mobility throughout the nanotubes and above all ensured an efficient synergetic effect between $WO_3$ and $TiO_2$ nanotubes.

## 4. CONCLUSION

The nanotubular TNT and tungsten trioxide-loaded TNT (WTNT) were successfully fabricated via anodization-annealing and electrodeposition method respectively. WTNT/–0.65 V synthesized in an adjusted solution pH of 1.5 had exhibited the highest PEC performance ($\eta$ = 9.63%) compared to other WTNT samples and was even 6 times better compared to blank TNT ($\eta$ = 1.65%). This was believed to be based on several factors. First, the high amount of deposited tungsten trioxide with good morphology had minimized the TNT's top coverage and maximized the $WO_3$-$TiO_2$ surface contact. Second, the crystallinity of the samples had allowed efficient electron mobility. Third, the visible light reactivity of $WO_3$ had widened the light spectrum absorption of the TNT. Fourth, the band gap narrowing effect induced by $WO_3$ had enhanced the charge separation of TNT. Further investigation should be made on the effectiveness of the electron-hole separation of the resulting WTNT via X-Ray Photoelectron Spectroscopic (XPS) analysis.

ACKNOWLEDGEMENTS
This study was financially supported by Universiti Teknologi MARA, through the Lestari Grant (600-IRMI/DANA KCM 5/3/LESTARI (192/2017).

## References

1. Y. Zhao, N. Hoivik, and K. Wang, *Nano Energy*, 30 (2016) 728–744.
2. P. Benjwal and K. K. Kar, *Mater. Chem. Phys.*, 160 (2015) 279–288.
3. R. Beranek and H. Kisch, *Electrochem. commun.*, 9 (4) (2007) 761–766.
4. T. A. Aljohani and A. K. Almutairi, *Int. J. Electrochem. Sci.*, 11(8) (2016) 6848–6861.
5. E. A. Al-Arfaj, *Superlattices Microstruct.*, 62 (2013) 285–291.
6. J. Liu, B. Liu, Z. Ni, Y. Deng, C. Zhong, and W. Hu, *Electrochim. Acta*, 150 (2014) 146–150.
7. M. N. Shaddad, M. a Ghanem, M. S. Alhoshan, and J. P. Singh, *Int. J. Electrochem. Sci.*, 8 (2013) 2468–2478.

8. S. Sreekantan, S. Mohd, C. Wei, and T. Wah, *Mater. Sci. Semicond. Process.*, 26 (2014) 620–631.
9. Y. Li, B. Wang, S. Liu, X. Duan, and Z. Hu, *Appl. Surf. Sci.*, 324 (2015) 736–744.
10. H. Sun, B. Dong, G. Su, R. Gao, W. Liu, L. Song, & L. Cao, *Appl. Surf. Sci.*, 343 (2015) 181–187.
11. A. S. Martins, P. J. M. Cordeiro-junior, L. Nuñez, M. Roberto, and D. V. Lanza, *Electrocatalysis*, 4 (2016).
12. M. M. Momeni and Z. Nazari, *Ceram. Int.*, 42 (7) (2016) 8691–8697.
13. M. M. Momeni and I. Ahadzadeh, *Mater. Res. Innov.*, 20 (1) (2016) 44–50.
14. M. Xiao, L. Wang, X. Huang, Y. Wu, and Z. Dang, *J. Alloys Compd.*, 470 (1–2) (2009) 486–491.
15. J. Gong, W. Pu, C. Yang, and J. Zhang, *Catal. Commun.*, 36 (2013) 89–93.
16. M. M. Momeni, Y. Ghayeb, and S. Gheibee, *Ceram. Int.*, 43 (1) (2017) 564–570.
17. W. D. Shahizuan and Y. Mohd, *J. Sci. Technol.*, 32 (2012) 49.
18. Y. C. Lim, Z. Zainal, W. T. Tan, and M. Z. Hussein, *Int. J. Photoenergy*, 2012 (2012).
19. S. Yoriya and N. Bao, *Int. J. Electrochem. Sci.*, 9 (12) (2014) 7182–7197.
20. S. Norsafurah, A. Malek, and Y. Mohd, *In Advanced Materials Research*. 748 (2013) 144-149. Trans Tech Publications. .
21. S. Yoriya and A. Chumphu, *Int. J. Electrochem. Sci.*, 11 (11) (2016) 9088–9099.
22. Y. Djaoued, S. Balaji, and R. Brüning, *J. Nanomater.*, 2012 (2012).
23. T. Zhu, M. N. Chong, Y. W. Phuan, J. D. Ocon, and E. S. Chan, *J. Taiwan Inst. Chem. Eng.*, 61 (2016) 196–204.
24. A. C. Marques, L. Santos, M. N. Costa, J. M. Dantas, P. Duarte, A. Gonçalves, ... & E. Fortunato, *Sci. Rep.*, 5 (2015) 1–7.
25. Y. R. Smith, B. Sarma, S. K. Mohanty, and M. Misra, *Electrochem. commun.*, 19 (1) (2012) 131–134.
26. S. Nadzirah, K. L. Foo, and U. Hashim, *Int. J. Electrochem. Sci.*, 10 (7) (2015) 5498–5512.
27. L. Jeffery, K. Hang, H. Abdul, and M. Bin, *Ceram. Int.*, 40 (10) (2014) 16015–16021.
28. L.-Y. Lin, M.-H. Yeh, C.-Y. Chen, R. Vittal, C.-G. Wu, and K.-C. Ho, *J. Mater. Chem. A*, 2 (22) (2014) 8281.
29. Y. C. Hsiao, Y. H. Tseng, and C. C. Hu, *Appl. Catal. B Environ.*, 147 (2014) 617–623.
30. M. M. Yusoff, M. H. Mamat, M. F. Malek, A. B. Suriani, A. Mohamed, and M. K. Ahmad, *Mater. Lett.*, 164 (2016) 294–298.
31. P. Roy, S. Berger, and P. Schmuki, *Angew. Chemie - Int. Ed.*, 50 (13) (2011) 2904–2939.
32. M. M. Momeni, Y. Ghayeb, and Z. Ghonchegi, *Ceram. Int.* 41 (7) (2015) 8735–8741.
33. M. M. Momeni and Y. Ghayeb, *Ceram. Int.*, 42 (6) (2015) 7014–7022.
34. Q. Wang, R. Jin, M. Zhang, and S. Gao, *J. Alloys Compd.*, 690 (2017) 139–144.
35. Q. Wang, J. Qiao, X. Xu, and S. Gao, *Mater. Lett.*, 131 (2014) 4–6.
36. Y. Yin, E. Liu, H. Li, J. Wan, J. Fan, X. Hu, ... & C. Y. Pu., *Ceram. Int.*, 42, 8 (2016) 9387–9395.
37. W. Sun, D. Wang, Z. U. Rahman, N. Wei, and S. Chen, *J. Alloys Compd.*, 695 (2017) 2154–2159.
38. M. M. Momeni, *Rare Met. Mater. Eng.*, 45 (11) (2016) 2779–2783